

Retrospective Theses and Dissertations

1985

Protein Concentration Elevations in Mouse Lung Following Sudden Transient Cephalad (+Gz)

Charles J. Gutierrez
University of Central Florida

 Part of the [Medicine and Health Sciences Commons](#)
Find similar works at: <https://stars.library.ucf.edu/rtd>
University of Central Florida Libraries <http://library.ucf.edu>

This Masters Thesis (Open Access) is brought to you for free and open access by STARS. It has been accepted for inclusion in Retrospective Theses and Dissertations by an authorized administrator of STARS. For more information, please contact STARS@ucf.edu.

STARS Citation

Gutierrez, Charles J., "Protein Concentration Elevations in Mouse Lung Following Sudden Transient Cephalad (+Gz)" (1985). *Retrospective Theses and Dissertations*. 4785.
<https://stars.library.ucf.edu/rtd/4785>

PROTEIN CONCENTRATION ELEVATIONS IN MOUSE LUNGS
FOLLOWING SUDDEN TRANSIENT CEPHALAD (+G_Z) ACCELERATION

BY

CHARLES JOSEPH GUTIERREZ
A.A., Hillsborough Community College, 1974
B.A., University of Tampa, 1976
B.S., University of Central Florida, 1982

THESIS

Submitted in partial fulfillment of the requirements for the
Master of Science degree in Health Science
in the Graduate Studies Program of the College of Health
University of Central Florida
Orlando, Florida

Spring Term
1985

ABSTRACT

Laboratory and feral lineages of mice were subjected to cephalad (+G_z) accelerations, for 1.8 seconds, aboard a solid fuel rocket. Spectrophotometric analysis of bronchoalveolar lavage retrieved post launch revealed significant ($p < .001$) elevations of protein in the lungs of experimental mice. Sudden transient imposition of a mean +G_z acceleration of $6.22 \pm .47$ (SD) G, at lift-off, may have induced hypervolemia of basilar pulmonary microvasculature with concomitant migration of fluid and protein from intravascular to juxta-alveolar perivascular compartments. Exudates may have entered bronchiolar airways subsequently gravitating toward alveoli.

ACKNOWLEDGEMENTS

The following individuals are acknowledged for their contributions on behalf of this research project. I am indebted to:

Daniel J. Crittenden, Ph.D., major professor and graduate committee co-chairman who as mentor taught me research techniques, philosophy of science and the importance of critical independent scientific investigation. As co-investigator, he provided me with superb assistance and consultation throughout the research effort.

J. Stephen Lytle, M.S., R.R.T., graduate committee member whose enthusiasm and inquiries regarding the progress of the research were very helpful. Because of his confidence in me I was given the opportunity to serve a graduate teaching assistantship that made financial support for the research project possible.

Louis J. Acierno, M.D., F.A.C.C., graduate committee member whose consultations continually inspired me to redouble my commitment to a career in academic cardiopulmonary therapy.

John H. Armstrong, Ed.D., graduate committee member who served as my initial graduate advisor and whose interest and encouragement were appreciated.

Thomas S. Mendenhall, Ph.D., graduate committee co-chairman whose expertise concerning administrative and educational degree requirements enabled me to proceed on schedule toward the charter MSHS degree.

Ruth Chalfant, Respiratory Therapy Program secretary whose patient attention to detail and superb typing capabilities are in evidence throughout this thesis.

Daniel R. Dukesherer, B.S., chemist whose consultations regarding methods and materials in chemical analyses were invaluable.

L. Timothy Worrell, M.P.H., R.R.T., Respiratory Therapy faculty member whose interest and encouragement throughout the project were very appreciated.

Marilyn Kangelos, M.S., M.T. (ASCP), Director of the Medical Technology Program, who allowed us to use equipment and space in the University of Central Florida Medical Technology Lab.

Sharon E. Douglass, M.S., R.R.T.(C), Respiratory Therapy faculty member whose interest and encouragement throughout the endeavor were greatly appreciated.

Michael F. Borman, computer program author with whom consultations resulted in the development of an optimum rocket flight computer program that was essential to the success of the research effort.

Pragna Mehta, technician, University of East Carolina, whose guidance regarding the sequence of mathematical calculations needed to obtain protein concentration per gram lung was very appreciated.

Linda C. Malone, Ph.D., University of Central Florida Institute of Statistics, whose guidance regarding employment of appropriate statistical analyses was greatly appreciated.

David E. Lougee, animal facility technician whose humane care for our research animals was greatly appreciated.

Candie F. Stewart, Editorial Assistant, University of Central Florida Library, whose careful inspection of this thesis was greatly appreciated.

The Respiratory Therapy Program at the University of Central Florida for allowing me to use materials, equipment and space in the Cardiopulmonary Research Lab.

The Department of Biological Sciences at the University for allowing us to use their animal facility as quarters for our animal colonies.

Carmen I. Delmoral, nursing student, Valencia Community College, who as research assistant provided me with invaluable help at the launch site and in the laboratory. Her devotion, encouragement and interest throughout this endeavor were very appreciated.

Florencio and Delia Gutierrez, my parents, who demonstrated the importance of dedication to the pursuit of excellence in scholarship and whose sacrifices, guidance, encouragement, confidence, patience and love have enabled me to pursue this goal.

TABLE OF CONTENTS

LIST OF TABLES	viii
INTRODUCTION	1
Alterations in Cardiopulmonary Physiology Associated With +G _z Acceleration	1
Past Research	1
Current Research	1
+G _z Acceleration	2
Blood Mobility Alterations	3
Cardiovascular Alterations	4
Pulmonary Blood Flow Alterations	4
Alveolar Configurations and Pleural Pressure Alterations	6
Ventilatory Alterations	7
Development of Hemodynamic Pulmonary Edema Associated With +G _z Acceleration	8
Anatomical Considerations	8
Murine Alveolar Septum	8
Endothelial Intercellular Junctions	8
Alveolar Interstitial Spaces	10
Epithelial Intercellular Junctions	12
Murine Juxta-alveolar Anatomy	13
Endothelial Intercellular Junctions	14
Peribronchiolar Regions	15
Epithelial Intercellular Junctions	15
Physiological Considerations	16
Pulmonary Edema Development	16
High Pressure Edema	16
Increased Permeability Edema	17
Selected Factors Affecting Pulmonary Edema Development	17
Alveolar Hypoxia	18
Mechanical Factors	19
Increased blood flow velocity gradients	19
Experimental effects	19
Neurogenic pulmonary edema	20
Lavage Protein	20

METHODS AND MATERIALS	22
Equipment	22
Rocket	22
Solid Fuel Engine	22
Launch Control System	23
Animals	23
Experimental Protocol	25
Prelaunch Preparations	25
Hardware Preparation	26
Animal Preparation	27
Launch Procedures	27
Recovery Procedures	28
Surgical Procedures	28
Lung Evacuation	29
Lavage Procedures	30
Protein Assay	31
Data Processing	33
RESULTS	35
Acceleration Data	35
Powered Flight	35
Coast-Ascent	38
Coast-Descent	38
Physiological Data	39
Animal	39
Protein Assay	40
DISCUSSION	42
Prelaunch	42
Animal Stress	42
Abdominal Binders	43
Hypoxemia	44
Launch	45
Powered Flight	45
Coast-Ascent	49
Coast-Descent	50
CONCLUSION	52
APPENDICES	
APPENDIX A	56
APPENDIX B	64
LITERATURE CITED	68

LIST OF TABLES

TABLE

I	Periodic Flight Parameters for Experimental Mice	36
II	Bronchoalveolar Protein and Fluid Content	41

INTRODUCTION

Alterations in Cardiopulmonary Physiology Associated With +G_z Acceleration

Past Research

In 1952 mice were accelerated in V-2 and Aerobee rockets by the U.S. Army in New Mexico (1). The animals reached heights of 80 miles at speeds over 2,000 miles per hour. Some physiologic parameters were measured but data regarding pulmonary hemodynamics were not recorded. These flights may not have addressed questions regarding effects of +G_z acceleration on murine pulmonary microvasculature. Lung wet weight/body weight ratios and bronchoalveolar protein content were not reported, and the presence or absence of pulmonary edema was not noted.

The purpose of this investigation was to determine if sudden transient cephalad +G_z acceleration might alter the microvasculature of mouse lung. Increased protein in bronchoalveolar lavage was measured for evidence of altered microvasculature. Data from these observations may provide a baseline for morphologic and physiologic studies in the future. The data may also have relevance in aerospace medicine.

Current Research

Experimental mice were subjected to sudden transient +G_z acceleration. Lungs were lavaged with saline and the recovered fluid analyzed spectrophotometrically for protein concentration. A Kruskal-Wallis H test for analysis of treatment effects and a multiple

comparisons procedure were used to evaluate the data (2,3). Intra-alveolar protein concentrations were greater in experimental mice than in control mice ($p < .001$). These data suggest pulmonary edema formation resulting from acceleration. An increased wet weight of the lung, usually found concomitantly with increased alveolar protein, was not seen in the present study. Possible mechanisms in sudden transient $+G_z$ acceleration that increase protein concentration without increasing lung weight will be discussed.

$+G_z$ Acceleration

Several excellent reports discuss physiologic and anatomic alterations in humans and animals subjected to acceleration. These reports include data from aircraft (4,5) and centrifuge experiments (6). Centrifuges have some advantages in that acceleration forces can be precisely controlled and instrumentation for recording data is easily accommodated. Roentgenographic machines and whole animal freezing units (7) have been placed aboard centrifuge gondolas along with the experimental subject.

Acceleration forces of 5 to 6G may occur over a period of several seconds during human rocket acceleration (8). Examination of the acceleration profile of astronaut John Glenn's powered flight phase showed that more than 120 seconds were required to reach 6G. A spectrum of physiologic alterations, including hemodynamic pulmonary edema, may occur during gradual, prolonged accelerations of this kind. Sudden transient acceleration as employed in the present study may yield physiologic and anatomic changes resembling those normally

seen following gradual long-term acceleration for the same reason that large doses of drugs are administered to mice over short periods to approximate the consequences of long-term administration.

Blood Mobility Alterations

The responses of pulmonary microvasculature, blood, airways and alveoli to gravity vary as a function of their location within the hemithoraces. The specific gravity of intrapulmonary gases is practically zero. Therefore, gas pressures in pulmonary airways, alveolar sacs and alveoli are equal to ambient atmospheric pressure provided that no airway obstruction is present (8,9). Lung tissue has a low density ranging from 0.2 to 0.3 gm/cm³ and will not readily distort caudally if exposed to +G_z acceleration (10). In contrast, blood in pulmonary microvascular compartments has a density of 1.06 gm/cm³, making it very responsive to gravitational gradients (10).

Blood has been documented as the most mobile organ (8). Examples of how quickly blood flow alterations occur in humans in response to acceleration include the onset of loss of vision, hearing and consciousness in as early as four to six seconds following exposure of +4 to 6G_z (11). Lindberg (5) has suggested that disturbances of vision and consciousness may occur if +G_z acceleration for more than three seconds at a rate of onset of 1 to 2G per second is maintained. Dimming of peripheral vision at a mean of 3 to 4G for more than three seconds, loss of peripheral vision at 3.5 to 4.5G, and loss of central vision at 4 to 5G have been reported (5). These symptoms may have been

due to stagnant hypoxia of the retina (8,12). In some mammals hearing and consciousness are lost during accelerations of 0.5 to 1G in excess of G at which central vision is lost (5).

Cardiovascular Alterations

Exposing animals to $+G_z$ acceleration is known to reduce cardiac output in man and dog. At $+3G_z$, cardiac output decreases by about 20 percent (5), and heart rate increases by 56 percent (5). Burton et al. (4) have found heart rates to be directly proportional to G magnitude and duration, provided the former is less than 6G and the latter less than 15 seconds. The frequency of occurrence of Premature Ventricular Contractions (PVC) was shown to increase as G increased from +7 to $9G_z$ (4). Tachycardia giving rise to dysrhythmias during acceleration may be secondary to excessive sympathetic activity, changes in cardiac orientation and configuration, and alterations in cardiac filling leading to ischemia with S-T segment depression (4).

Increased total peripheral resistance has been documented following baroreceptor response to $+G_z$ stress (13,14). $+G_z$ acceleration results in pooled blood in vasculature below the heart. Decreases in venous return, cardiac output and blood pressure stimulate baroreceptors to elevate pressures above 300 mm Hg (4) and induce tachycardias ranging from 170 to 205 beats/minute (15).

Pulmonary Blood Flow Alterations

Blood flow distribution in microvasculature of isolated dog lung has been identified according to relative arterial, venous and alveolar

pressures (16). The most cephalad, zone 1, receives no blood flow due to low arterial pressure. In zone 2, arterial pressure exceeds alveolar pressure and blood flow is directly proportional to the arterial-alveolar pressure differential (17). In zone 3, arterial and venous pressures exceed alveolar pressure and blood flow is directly proportional to the arterial-venous pressure differential. The upper limit to which blood rises in human pulmonary microvasculature during exposure to $+G_z$ acceleration has been examined by xenon-lung scan (10). Scans revealed that humans exposed to an acceleration of $+1G_z$ would have no perfusion within 4.5 cm from the lung apex, leaving approximately 13 percent of ventilated lung volume unperfused. When acceleration is increased to $+2G_z$ the unperfused region moves caudally so that no perfusion is available within 9.7 cm from the lung apex and approximately 29.5 percent of the ventilated lung volume is not perfused. At $+3G_z$ the unperfused zone regresses further caudally such that no perfusion is present within 14.2 cm from the lung apex, representing 45 percent of ventilated, unperfused lung volume (10). The most caudal five centimeters of lung remained perfused regardless of $+G_z$ magnitude. Apex to base distance in human lung is approximately 30 cm (7). Blood flow rate at various levels of the upright lung has been found to increase linearly during acceleration as lung base is approached and the rate of increase is directly proportional to $+G_z$ magnitude (10).

During $+G_z$ acceleration the high ventilation-perfusion (\dot{V}_A/\dot{Q}_C) ratio at the lung apex rises until at $+3G_z$, it approaches infinity (18).

Simultaneously, the low \dot{V}_A/\dot{Q}_C ratio at the lung base declines further. Arterial hypoxemias in subjects breathing air while subjected to $+G_z$ acceleration have been attributed to right to left shunting. Jones et al. (19) demonstrate that airway collapse may occur in dependent lung during $+G_z$ acceleration and may be responsible for trapping gas in alveoli. Perfusion around these alveoli give rise to absorption atelectasis and hypoxemia (10).

Alveolar Configurations and Pleural Pressure Alterations

During sudden transient $+G_z$ acceleration, size and patency of alveoli in superior and dependent regions of the lung are not significantly affected by the weight of the pulmonary tissue but by intrapleural and intravascular pressure alterations in these regions.

In zero G environments, intrapleural pressures are equally negative throughout the pleural space (8). Examinations of arterial and venous pressures exhibit no vertical pressure gradients within the hemithoraces although arterial pressures exceed venous pressures, maintaining pressure gradients that sustain blood flow. At $+1G_z$, apical pleural pressures become more negative than those at the midthoracic pelura which are more negative than those at the base of the pleural space. Vertical pressure gradients between arterial and venous hydrostatic columns are present and basilar pressures exceed apical pressures in arterial and venous circuits (5). At $+5G_z$ there is a fivefold accentuation in intrapleural pressures so that apical pressures become markedly negative while basilar pressures become markedly positive (8). Fivefold changes also occur in

hydrostatic pressures such that apical arterial and venous pressures become markedly negative while basilar arterial and venous pressures become markedly positive (9).

Animals employed in $+G_z$ accelerations have had abdominal binders placed to help maintain adequate cerebral perfusion pressures. Data suggest that differences between sizes of apical and basilar alveoli may be accentuated when binders are used (7). Binders raise pleural pressure above airway pressure, collapsing some small airways in dependent regions and preventing escape of gas from alveoli and initiating atelectasis. Hughes et al. (20) suggest that reductions in volume of basilar alveoli may have increased interstitial pressure within pulmonary parenchyma, increasing vascular resistance in dependent regions and decreasing blood flow.

Ventilatory Alterations

Ventilation rates in humans increase 3.5-fold as acceleration increases from +1 to $7G_z$ (4). $PaCO_2$ changes minimally and may be due to increased pulmonary dead-space/tidal volume (V_D/V_T) ratio as blood pools in dependent lung. Tidal volume (V_T) tends to increase but is limited as higher G levels are imposed. Burton (4) has suggested that this limitation may be due to the increased weight of the thoracic wall during acceleration.

Glaister (21) has found significant falls in vital capacity (VC) among air breathing subjects at $+6G_z$. Burton (4) has implied that VC reductions result from decreases in pulmonary parenchymal compliance due to altered surface tension in alveoli and/or very small airways.

Development of Hemodynamic Pulmonary Edema Associated
With +G_z Acceleration

Anatomical Considerations

Murine Alveolar Septum. Alveolar septum has been proposed as a region where hemodynamic pulmonary edema may develop initially (22). Others have proposed peribronchiolar connective tissue sites as regions where edema develops initially (23). The site of edema formation varies with animal model and experimental conditions. Regardless of where edema begins, fluid and protein must first migrate via endothelial intercellular junctions.

Endothelial Intercellular Junctions. Claude and Goodenough (24) have examined permeability characteristics of intercellular junctions in freeze-fractured tissue from many sources. They conclude that junction permeability varies as a function of its number of strands rather than its width. Schneeberger and Karnovsky (25) have suggested that endothelial junctions comprise one to three rows of intramembranous particles and may be permeable to water-soluble solutes. Using uranyl acetate staining, they have found intramembranous particles, identified as maculae occludentes, between murine pulmonary endothelial cells (26). Staehelin and Hall (27) have described the particles as button-like intercellular contacts. Adjacent cell membranes within each macula are parallel and separated by 300 angstroms. The Central Stratum is a filament bisecting the intercellular space. Disk-shaped plaques are close to the cytoplasmic surface of each cell membrane. Tonofilaments 100 angstroms wide

connect to cytoplasmic plaques and extend into cytoplasm as a tensile structural framework. Transmembrane linkers arise from the cytoplasmic plaque, project into intercellular space and connect to the Central Stratum in a staggered pattern. Transmembrane linkers connect tonofilaments of adjacent cells, creating a tensile infrastructure shared by the entire endothelium.

Murine pulmonary capillary endothelial junctions have been found to contain discontinuities through which cytochrome c (molecular diameter--15 angstroms) can pass within seconds of being injected with a small volume of saline. Pulmonary capillary endothelial junctions have been found to become permeable following transient increases in intravascular volume (28) or hydrostatic pressure (29). Increased surface area of zone 3 pulmonary capillaries due to increased intravascular pressures have been reported (30). This may accentuate discontinuities within maculae occludentes enabling fluid and protein to exude into true interstitium of alveolar septum.

Pietra et al. (29) suggest that intravascular pressure may play a role in macromolecular transport along endothelial junctions. Proteins with molecular weights exceeding horseradish peroxidase (molecular weight--40,000) are not able to negotiate murine pulmonary endothelial junctions (31). Hemodynamic forces become evident when hemoglobin (molecular weight--64,500) is infused into dog lung at 50 mm Hg. Under these pressures, endothelial junctions stretch and become permeable to hemoglobin (29).

Schneeberger and Karnovsky (28) have calculated a murine pulmonary endothelial pore radius of 40 to 58 angstroms. The radius allows passage of the macromolecular tracer horseradish peroxidase (HRP) which has a molecular diameter of 50 angstroms (32). Albumin has a molecular diameter of 38 angstroms (33) and may also pass via endothelial pores especially during transient hypervolemia. Schneeberger and Karnovsky (28) have reported endothelial junction widths in noninjected (normovolemic) control mice to be 41 ± 1 (SE) angstroms while junctions of injected (hypervolemic) mice are 45 ± 2 (SE) angstroms. Junctions with cylindrical radii of 45 angstroms due to hypervolemia, have a slit width of 55 angstroms (34).

Mean blood volume in adult mice is 1.5 ml (35). When Schneeberger and Karnovsky (28) injected 5 mg HRP in .05 ml saline, the latter represented 3.5 percent of the animal's blood volume and HRP was confined to intravascular space (26). When 5 mg HRP was injected in 0.5 saline, this 35 percent of the blood volume induced a transient fluid overload that stretched endothelial junctions. Ninety seconds post injection, HRP passed through adluminal and abluminal ends of endothelial junctions and into endothelial basement membrane (28). These results suggest that hypervolemia may elevate microvascular blood pressures above normal (5 to 15 mm Hg), expanding endothelial junction diameter (28).

Alveolar Interstitial Spaces. Alveolar septa comprise capillary endothelium, alveolar epithelium with accompanying basement membranes, and an interstitium (36) with two distinct regions (37).

The pseudointerstitium consists of fused basement membranes from endothelia and epithelia; comprises 50 percent of the alveolar surface; and allows optimum gas exchange (22,37,38). Barrier thicknesses less than 0.5 micron represent pseudointerstitial spaces (38). HRP accumulation within pseudointerstitium has been found without increased interstitial volume (26). Karrer (36) has suggested that fused basement membranes may be joined by a three-dimensional collagen fibril network preventing increased interstitial volume.

True intersitium has been found to vary with species and to contain fibroblasts, collagenous and elastic fibrils (37,38). True interstitial spaces bounded by endothelium and epithelium may be confluent with larger interstitial spaces bounded by epithelium of juxtaposed alveoli. Barrier thicknesses in excess of 0.5 micron represent true interstitial spaces (38).

Connective tissue fibers in true interstitium form a fiber continuum that extends from axial structures such as bronchioles and pulmonary arteries to peripheral structures such as pleura or interlobular septa (37,38). A minimal pseudointerstitial thickness of 800 angstroms is present in most mammals (38). However, dimensions of true interstitium vary according to species. As lung size decreases, true interstitium becomes narrower due to a decreased population of connective tissue fibers (38). The axial component of the fibrous continuum extends into alveolar entrance rings (alveolar ducts). The peripheral component extends into pulmonary parenchyma. Both components are connected and anchored by connective tissue fibers

residing in the true interstitium (39). Anchoring fibers interlace with capillaries to form a three-dimensional polyhedral infrastructure that extends throughout the pulmonary parenchyma. Interlaced fibers and capillaries in each septum join other septa at triple-line intersections (38).

Connective tissue fibers in true interstitium extend into interstitial fluid sumps situated in connective tissue sheaths that encircle juxta-alveolar airways and blood vessels. Lymphatic capillaries have been demonstrated exclusively within juxta-alveolar regions and not in true interstitium of alveolar septa (28). A continuous interstitial space beginning in true interstitium extends into fluid sumps in juxta-alveolar regions containing lymphatic capillaries. Weibel and Bachofen (37) have suggested that any fluid within the continuous interstitium would move toward lymphatics along negative pressure gradients.

Fibroblasts in true interstitium may regulate compliance (40). Fibroblast processes attach firmly to alveolar epithelial basement membranes and may restrict septal space widening during episodes of edema (37).

Epithelial Intercellular Junctions. Schneeberger and Karnovsky (26) compared intercellular clefts of murine alveolar epithelial cells with those of endothelial cells and found the former were longer and more convoluted than the latter. Fused regions discovered toward the adluminal end of epithelial intercellular clefts were zonulae occludentes (25). The radius of this junction was 6 to 10 angstroms

and therefore smaller than maculae occludentes of endothelial cells (28).

Relative impermeability of zonulae occludentes has been demonstrated by injection 5 to 6 mg HRP dissolved in 0.5 ml saline. At 90 seconds post injection, alveolar epithelial clefts are devoid of HRP. When HRP extends into the intercellular cleft, it does not proceed into the adluminal portion of the cleft (26). Alveolar epithelial junction integrity was further challenged by doubling the amount of HRP and its diluent. Mice were given 10 mg HRP in 1.0 ml saline inducing sudden hypervolemia. At five minutes post injection, no HRP could be found in alveolar epithelial junctions (41).

Alveolar epithelial junctions are comprised of three to six highly (25) and evenly (27) interconnected sealing strands. Freeze-fracture studies have found sealing strands lying toward the apex of cells and within rather than between juxtaposed cell membranes. Each strand may be composed of two rows of tightly packed globular membrane proteins from which filaments arise and arborize into the cytoplasm (27). Splitting the epithelial membrane along its center exposes globular proteins within the bilipid layer (25). Local rupturing of several sealing strands in an epithelial junction has a negligible effect on overall seal tightness (27).

Murine Juxta-alveolar Anatomy. Experimental data suggest that sudden transient, hemodynamic edema may accumulate within peribronchiolar regions, later appearing in alveolar interstitial regions (23). Alternate data suggest that peribronchiolar regions become edematous without concomitant alveolar interstitial involvement (41).

Endothelial Intercellular Junctions. Yoneda (41) administered 10 mg HRP dissolved in 1.0 ml saline to mice in order to induce acute hypervolemia. HRP precipitate was found intravascularly 20 seconds post injection. By two minutes post injection, HRP had traversed endothelial junctions of small peribronchiolar arteries and by five minutes had induced peribronchiolar tissue widening. Simultaneously bronchiolar epithelial clefts, including the adluminal segment, were found completely filled with HRP. In capillary endothelial clefts, HRP was found well after it had passed through endothelial junctions of small peribronchiolar arteries. Cottrell et al. (22) have studied hemodynamic pulmonary edema in dogs and suggest that interstitial fluid may not arise from pulmonary capillaries but from larger vessels.

Contractile myofibrils within cells comprising endothelium of small peribronchiolar arteries have been proposed to explain why HRP negotiates arterial endothelial clefts quicker than capillary endothelial clefts (42). Contraction of the myofibrils are thought to increase the radii of intercellular junctions. After HRP penetrates intercellular clefts in arterial endothelium, it proceeds through endothelial basement membrane at myoendothelial junctions, passes through intercellular spaces of smooth muscle cells in medial layer and reaches perivascular space (41,43).

Pinocytotic vesicle chains are transendothelial channels through which enzymatic tracers may migrate. Vesicles may play a minimal role in perivascular edemagenesis because they are not as plentiful as intercellular clefts (41). Epithelial vesicles filled with HRP have not been found to discharge their contents into alveolar air space

casting doubt on the role played by these vesicles in transepithelial transport of fluid and protein (26).

Peribronchiolar Regions. Edema may accumulate perivascularly and peribronchiolarly (44). Erdman (45) has found albumin concentration in pulmonary lymph of standing sheep to be 84 percent of serum concentration. Lymph draining peribronchiolar interstitial fluid from septal regions may have normally high protein concentrations that become higher during acute hypervolemia.

Epithelial Intercellular Junctions. HRP appears in intercellular clefts of bronchiolar epithelial cells in direct communication with bronchiolar air space. This has been interpreted by Yoneda (41) as indicating the ability of HRP to leak through clefts without being impeded by the cleft's adluminal segment. In contrast, alveolar epithelium did not allow free passage of HRP into alveolar air space (26,41). The reason for HRP's easy passage into bronchiolar lumen is not known. One speculative possibility is that bronchiolar cells have fewer apical sealing strands than the three to six found in alveolar epithelium (25). Alternatively, cross linkages between the strands may be irregular. Less cross linking in strands could make cells less resistant to deformity from peribronchiolar fluid accumulation following acute hypervolemia. Few cross linkages have been reported among cells that expand to secrete a mucous product (27). The presence of secretory Clara cells at the bronchiolar epithelial level is well documented (39).

Physiological Considerations

Pulmonary Edema Development. Causes of pulmonary edema include increased microvascular hydrostatic pressure and/or increased vascular permeability. Obstructed lymphatic drainage and decreased vascular oncotic pressures usually result in pleural effusion (46). Pulmonary edema may be classified physiologically as hydrostatic (high pressure) or permeability (low pressure) forms and anatomically as interstitial or alveolar forms. To reach alveolar or bronchiolar air spaces, fluid and solutes must cross endothelial membranes, flow through interstitial space without draining into lymphatics and cross epithelial membranes (46).

Transvascular fluid balance is characterized by the Starling equation: $\dot{Q} = K [(P_{mv} - P_{pmv}) - \sigma (\pi_{mv} - \pi_{pmv})]$ where \dot{Q} is net transvascular filtration rate, K is fluid conductance via microvascular wall, P is hydrostatic pressure in microvascular (mv) lumen and in perimicrovascular (pmv) interstitial fluids, σ is microvascular protein reflection coefficient, and π is osmotic pressure in mv lumen and pmv interstitial fluids (46).

High Pressure Edema. Lymph flows constantly even when microvascular pressures are not elevated. During steady states the Starling equation is positive, indicating a tendency toward filtration. Increased intravascular pressure is attended by increased filtration. Rising protein reflection coefficients seen with increased microvascular pressure indicate restricted transendothelial protein leakage. An

association between low protein concentrations and edema fluids from high pressure edema has been reported (47). Elevated microvascular pressure may wash out perimicrovascular proteins resulting in increased osmotic pressure gradient from vessel lumen to the outside. The osmotic effect opposes the hydrostatic pressure difference, pulling fluid into the vessels. This protective negative feedback mechanism may be 50 percent efficient so for each 20 cm H₂O increase in hydrostatic pressure, osmotic pressure increases 10 cm H₂O (46). Under these conditions some exudation of protein and fluid will occur.

Increased Permeability Edema. Endothelial membrane damage tends to increase fluid conductance (K) and to decrease protein reflection coefficient (σ). The hallmark of increased permeability edema has been found to be high protein concentration in edema fluid (48). Lymph albumin concentration increases due to decreases in protein reflection and because pathologically disrupted interstitial spaces alter water and albumin travel rates through interstitium. In unremarkable interstitium albumin enters 50 percent of the space available for fluid (49). Damaged interstitium may be unable to exclude albumin from interstitial matrix. High interstitial hydrostatic pressure may induce fluid flow across normal airway epithelium (50) leading to antegrade filling of alveoli (51).

Selected Factors Affecting Pulmonary Edema Development. Sympathetic stimulation from nonspecific stresses has been found to acutely alter pulmonary microvascular size and permeability and may affect

fluid and protein exchange (52). These changes appear particularly important in rat lung which Beckman (53) has found to have a very low threshold of stress response. Sympathetic nerves have been demonstrated in pulmonary microvessles with diameters as small as 30 μm (54). Sympathetic interactions with alpha adrenergic receptor sites are known to result in arterial microvascular constriction (55) leading to hydrostatic pressure alterations and increased endothelial permeability to proteins (56). Alpha adrenergic receptors mediate increases in vascular permeability by prompting histamine release from perivascular mast cells (57). Some investigators have suggested that sympathetics alter alveolar surfactants and increase alveolar protein content (58).

Alveolar Hypoxia. Whayne and Severinghaus (59) have subjected rats to hypoxic exercise by having them swim in 36°C water while breathing 8 to 10 percent oxygen. Effects of hypoxia include pulmonary arteriolar constriction, increased cardiac output, lactic acidosis and hyperventilation. Left ventricular failure, pulmonary venous constriction and direct capillary injury are not found (59). Periarterial cuffs are the earliest indications of edema; with peribronchial and perivenous cuffs present to lesser degrees. Cuffs are not found around vessels less than 20 microns in diameter. Results reveal that in hypoxia edema leaks from arteries while capillaries are devoid of pressure and flow. Periarterial cuffing is due to arterial wall rupture from high pressure proximal to constricted arterioles (59).

Periarterial plasma or blood may form clots that obstruct lymphatics and exacerbate edema.

Alveolar hypoxia increases pulmonary arterial pressure and vascular resistance (60). Neumann et al. (61) demonstrate a shift in blood flow from dependent to apical regions in sheep lung. Pulmonary hypertension is characterized by increases in transmural pressures that dilate upper lung vessels redistributing flow to that region and increasing net transvascular filtration rate. Apical interstitial edema is difficult to confirm because lymph ducts drain basilar regions and are not in a position to reflect apical increases (62).

Mechanical Factors.

Increased blood flow velocity gradients. Acute increases in blood velocities induce alterations in endothelial cells. Hemodynamics along the blood-endothelial interface result in shearing stresses or convections that influence endothelium ionic milieu. Fry (63) has found that Evans-blue tagged albumin crosses endothelial surfaces that have been mechanically or electrochemically altered by increases in blood velocity gradients. Endothelium that endures increased hydraulic shear or turbulence concomitantly exhibits increases in infiltration of tagged albumin into intima. Exposure to shearing stresses above 379 ± 85 (SD) dynes/cm² induces endothelial cell swelling, deformation and dissolution (63).

Experimental effects. Isolated lungs have been artificially perfused to study microvascular filtration characteristics. Development of spontaneous edema has been reported. Morriss et al. (64) found

filtration rate per unit pressure drop across endothelium to be three times larger in isolated lung than in intact lung. Reasons for increased permeability include physical trauma to lung during excision, and interrupted blood and nerve supply.

Perfusate composition appears very important. Fisher et al. (65) were able to delay onset of pulmonary edema in isolated rat lung by adding bovine serum albumin to an electrolyte perfusate. A complete medium that supports the metabolic needs of endothelial and epithelial cells was found to keep isolated lungs free from edema (65).

Neurogenic pulmonary edema. Reports suggest that neurogenic pulmonary edema may occur due to increases in microvascular pressure and/or permeability. Sympathetic fibers that arise from the hypothalamus (66) are known to penetrate media of small pulmonary arteries (54). Protein rich alveolar edema has been found without simultaneously elevated arterial pressure (66,67,67). Van Der Zee et al. (69) interpret these data as evidence that neurogenic pulmonary edema is due to increases in permeability of capillary endothelium and airway epithelium without increases in hydrostatic pressure. Medullary and hypothalamic ischemia following intracranial hypertension increases sympathetic activity (66,67). Mechanical vibration has been found to yield sympathetic activity that results in sudden pulmonary damage (70).

Lavage Protein

Proteins from bronchoalveolar lavages may be endogenous or exogenous. Sueishi et al. (71) have induced duck antibodies against

rabbit pulmonary surface active material. Antibodies are separated from duck antisera and conjugated with HRP. Conjugates react diffusely with alveolar lining material, bronchiolar surfaces and tubular myelin. Findings indicate that phospholipid square patterns integrate and stabilize surfactant by being interspersed within a network of specific protein (71). Lamellar bodies, golgi complex, multivesicular bodies and endoplasmic reticulum within Type II cells exhibit conjugate accumulation, suggesting the role of Type II cells in synthesizing and secreting protein as part of surfactant (71).

Some investigators have proposed exogenous origins for lavage proteins. Hurst et al. (72) found no soluble protein in rabbit alveolar lining layers. Proteins, notably albumin, have easy access to air spaces of well perfused alveoli. Scarpelli et al. (73) hypothesize that proteins in surfactant are of intravascular origin. Clearance of blood from rat lung microvasculature results in an 80 percent decrease in albumin recovered by tracheal rinse (74). Alveoli rinsed directly by micropuncture, without rinsing trachea, yield a 70 percent decrease in bronchoalveolar lavage albumin concentration (74). Plasma constituents may have greater access to airway than to alveolar air spaces.

METHODS AND MATERIALS

Equipment

Rocket

The rocket accelerating experimental animals was a Maxi Icarus single stage miniature rocket (Estes Industries, Penrose, Colorado). The rocket body was a spiral wound paper tube. Fins were made of balsa wood and the nosecone was plastic. The Maxi Icarus was chosen for its transparent plastic payload compartment with a volume in excess of 98 cc. Payload capacity was 80 grams. Total length of the launch vehicle was 75.6 cm and external diameter of body tube and payload compartment was 4.16 cm. Assembly of the rocket required a moderate amount of skill.

Solid Fuel Engine

The D12-7 solid fuel engine (Estes Industries, Penrose, Colorado) was selected to loft the rocket. These prefabricated engines comprised a cardboard casing into which clay nozzle, high thrust propellant, tracking smoke charge, ejection deployment charge, and clay retainer cap were placed. Engines were manufactured within exacting tolerance limits. Production quality control insured reproducible performance from one flight to the next. Engines were used for one flight only. Engines were 6.99 cm in length, 2.4 cm in diameter, and weighed 44 gms

of which 24.93 gms were due to weight of propellant. Engines produced impulses of 20 Newton-seconds with maximal thrust of 4.1 Kg and maximal lift weights of 226.8 gms. Maximal $+G_z$ acceleration forces developed on a 30 gm payload were 6.1G. Thrust durations were approximately 1.8 seconds followed by a time delay of 7 seconds (± 15 percent) before the recovery parachute was deployed. The seven second time delay was selected to minimize downrange drift.

Launch Control System

A launch control system assembled from a light switch, electrical extension cords, battery clamps and microclips provided power to ignite engines. Electrical cords were attached to the light switch. Battery clamps and microclips were attached to opposite ends of the cord. The electrical circuit was completed by attaching battery clamps to a 12 volt automobile battery and attaching microclips to Solar igniters (Estes Industries, Penrose, Colorado) inserted inside the rocket engine.

Animals

Male and female mice (Mus musculus domesticus) (75) weighing 12.25 to 47.68 gms were randomly selected from black and white strains available at the University of Central Florida Animal Facility and from white strains available at local stores. The total number of mice studied was 25. Eight control mice were not launched and were not placed in the rocket payload compartment. The six animals in the sham control group were placed into the payload compartment for five

minutes but were not launched. The 11 experimental animals were placed into the payload compartment of the rocket and launched, subjecting them to linear acceleration. Mouse confinement never exceeded five minutes. The independent variable was exposure of an animal to linear acceleration. Dependent variable was elevated protein in bronchoalveolar lavage of experimental mice.

Animals had physical examinations before being assigned to sample groups. Coats were examined for fur loss and parasites. Mucous membranes were examined for serosanguinous discharge, rubor and swelling. Ventilatory excursions and rates were noted. Animals with signs of prior combat were not employed in the experiment. Animals that self-sequestered or appeared infirmed were removed from the colony and disqualified from further participation.

Animals were placed on a nutrient regime of Rodent Blox (Continental Grain Company, Chicago, Illinois) and were given water ad libitum. Animals kept themselves well hydrated and hemoconcentration was not suspected (75). Animals were kept in the Cardiopulmonary Research Laboratory or Medical Technology Laboratory at the University of Central Florida, in plastic, well ventilated, sanitary, small rodent cages with wire tops. Ambient temperatures were kept slightly below 25°C and artificial lighting periods simulated regular circadian rhythms.

Experimental Protocol

Prelaunch Preparations

Prior to launch, information was obtained from the National Weather Bureau regarding wind direction and speed, temperature, humidity, presence of overcast and forecast. Wind direction and speed dictated the position of the launch tripod. All launches were carried out in accordance with the safety code of the National Association of Rocketry.

Before launch all rocket component weights were recorded. Some values were later inserted into a computer program (76) that calculated three flight parameters (Appendix A, p. 56). The body tube of the rocket was cleaned with a large test tube brush prior to each launch in order to prevent charge deposits from accumulating. Deposits would have increased rocket weight and diminished the ability of each engine to provide consistent acceleration between animals.

Each experimental, control and sham control animal was measured for length and width and placed into a preweighed cardboard box. Box and mouse were weighed on a Mettler P1210 Balance (Mettler Instrument Corporation, Princeton, New Jersey). A closed box improved weighing accuracy and minimized stress.

Enclosed animal, rocket, launch control system and field supply kit were placed in a Transport Module designed for the current project. Syringes, hypodermic needles, anesthetic, scalpels, blades, suture, tape, towels and saline were transported in a utility box (Akro-Mils,

Akron, Ohio). Launches were conducted in the southeastern quadrant of the University of Central Florida campus, Orlando, Florida.

Hardware Preparation. A launch tripod was placed three meters from an automobile whose battery was used to ignite the rocket fuel and whose body provided protection from rocket engine blast. The tripod supporting a launch rod and blast deflector (Estes Industries, Penrose, Colorado), enabled the rocket to be launched into the wind to minimize downrange drift. At no time was the angle from vertical greater than 10 degrees.

Six sheets of recovery wadding (Estes Industries, Penrose, Colorado) were placed into the body tube. The elastic shock cord and anchor were tested for strength. A 25.4 cm parachute (Estes Industries, Penrose, Colorado) was attached to the balsa nose block. Test flights had shown that a 25.4 cm parachute would allow a rocket lofting a payload of 45 gms to descend at a rate allowing recovery of the rocket in midair.

A Solar igniter was inserted in the engine's ceramic nozzle followed by a 5 mm sphere of wadding to stabilize the igniter. Approximately 1.5 turns of masking tape were applied to the nozzle end of the engine to assure a snug fit within the engine block. After slipping the rocket over the launch rod and setting it on the blast deflector, an index card was interposed between deflector and igniter to prevent short circuiting ignition wires.

Animal Preparation. Each animal was placed in a plastic film canister (Eastman Kodak, Rochester, New York) weighing 5 gms and containing a 10 mm opening at one end. The canister did not impede ventilatory excursions of the rib cage, but it was not known whether external respiration was quantitatively affected by canister application. Compression of abdominal contents may have imposed limitation on larger mice. A hemostat pulled the tail through the opening and around to the side of the canister where the tail was held in place with masking tape.

The canister oriented and maintained the animal vertically allowing effects of $+G_z$ acceleration on mouse pulmonary vasculature to be studied. Apexes of the lungs pointed toward the nose cone while bases, pointed toward the engine. The longitudinal pulmonary axes remained parallel with the vector of linear acceleration.

Launch Procedures

As recovery crews took positions, the canister containing the animal was placed in the payload compartment. A foam rubber ring with an external diameter of 4 cm, internal diameter of 2 cm and thickness of 1 cm, was placed over the snout and followed by a disk with an external diameter of 4 cm and a thickness of 1 cm. The ring and disk stabilized the snout and absorbed headward shocks. Cushions were porous and represented no obstruction to ventilation. No cushions were placed at the caudal end of the animal.

The nose cone was attached to the payload compartment and the switch turned on to ignite the engine. Launches were immediate linear

accelerations carrying mice to a mean height of 259.73 ± 8.23 (SD) meters and subjecting them to approximately 6.1G at lift-off.

Recovery Procedures

After recovering the rocket, the animal was removed from the payload compartment. Tail was untaped from the film canister side and the animal taken from the canister. Each mouse was examined for ventilatory excursions and rates. Mucous membrane color was noted as an index of perfusion and degree of blood pooled in lung base.

A dose (35 mg/kg body weight) of Ketalar (Park, Davis, and Company, Detroit, Michigan) was given intraperitoneally. Anesthetic efficacy was assessed by performing toe pinch tests and monitoring corneal reflexes.

Surgical Procedures

Time from recovering the mouse to beginning surgery was five to ten minutes. The anesthetized animal was placed supine on a folded paper towel with paws and snout taped to the towel in such a way that ventilation was not obstructed. Taping animal to a towel allowed the entire animal to be manipulated during surgery.

A midcervical incision was extended caudally to 5 mm below the diaphragm. Peritracheal fat and muscles were excised and trachea freed by blunt dissection. A midsternal incision was begun at the episternal notch of the manubrium and extended through the xiphoid process. Inducing bilateral pneumothoraces via the manubrium instead of the xiphoid was associated with decreased lavage leaks.

Retromanubrial fatty tissues may have allowed penetration of the rib cage without substantial pulmonary lacerations.

At the caudal end of the midsternal incision, bilateral incisions from the xiphoid were extended along intercostal muscles toward the vertebral column. Incisions were extended cephalad and parallel with the anterior edge of the lung. Incisions ended at midclavicle and excised bilateral triangularly shaped portions of the chest that allowed unencumbered access to heart and lungs. Damage to pulmonary parenchyma was graded on a scale of increasing severity from 0 to 6 (Appendix B, p. 64). Major vessels at the cardiac base were excised allowing the heart to be removed en bloc. After excising the superior aspect of the larynx, traction placed on the larynx and trachea allowed lungs to be freed from esophagus, vertebral column and diaphragm.

Lung Evacuation

Visceral pleura was washed with saline to remove blood. Lungs were blotted dry and weighed. Lungs were degassed following a version of the technique performed by Oyarzun and Clements (77). A 50 ml syringe, tygon plastic tubing and a pressure gauge (Marsh Instrument Company, Skokie, Illinois) were used in degassing lungs. Lungs were placed on moist gauze and inserted into the syringe followed by the plunger. After affixing gauge and tubing to syringe, the plunger was withdrawn thereby achieving an intrasyringe pressure of -381 mm Hg for 60 seconds. Lungs were evacuated to facilitate fluid flow into distal airways during lavage.

Lavage Procedures

Lavage apparatus was assembled from a 5 ml lock tip syringe (Pharmaseal Laboratories, Glendale, California), a K75 three-way stopcock (Pharmaseal Inc., Toa Alta, Puerto Rico), a 21 gauge, 3.8 cm hypodermic needle (Becton, Dickinson and Company, Rutherford, New Jersey) and 3 cm of Intramedic Non-Radiopaque Polyethylene Tubing (Clay Adams, Parsippany, New Jersey). After taking lungs from the 50 ml syringe, Intramedic tubing was used to intubate the trachea. Silk braided sutures (Ethicon Inc., Somerville, New Jersey) were tied over the cephalic end of the trachea and crosstied over the stopcock to prevent inadvertant extubation.

Lavage fluids were inserted according to lung weight as described by Oyarzun and Clements (77). Approximately 10 ml saline were inserted per gram lung. Three consecutive lavage insertions were carried out for each lung. Lavage fluid recovered after every first insertion was stored in an acid washed Nalgene bottle (Nalge Company, Rochester, New York). The second lavage fluid insertion was equal to the volume recovered in the first attempt. The third lavage fluid insertion was equal to the volume recovered in the second attempt. Each successive rinse was adjusted for the amount retained in the lung thereby preventing overdistension. All lavage obtained from the tracheobronchial tree and all fluid that leaked directly from parenchyma were combined for analysis. Leaked fluid was considered tracheobronchial tree injectate that recovered bronchoalveolar protein prior to leaking from a pulmonary rent. Pooled lavage was mixed and stored at 0°C until analysis.

Protein Assay

A protein assay kit, Catalog Number 500-0002, (Bio-Rad Laboratories, Richmond, California) was used to determine lung protein concentrations. The assay quantitated soluble proteins based on differential color changes that occurred as dye bound with various concentrations of protein. The Bio-Rad assay was faster and easier to employ than the Lowry protein determination method and yielded comparable results (78).

The Bio-Rad Assay Kit II consisted of one bottle of dye reagent concentrate containing 450 ml of dye solution, phosphoric acid and methanol. The kit also contained one vial of lyophilized bovine albumin as a standard of comparison for samples containing primarily albumin. The main protein in bronchoalveolar lavage may be albumin derived from intravascular compartment (74). Exactly 100 ml of dye reagent concentrate was added to 400 ml of high quality distilled water. Expected albumin concentration according to the label on the vial was 1.21 mg/ml.

A standard assay was performed by preparing seven dilutions of protein standards. In addition, a blank sample containing 5.1 ml saline and a sample containing 0.1 ml saline plus 5 ml dye reagent were prepared. Dilutions of lyophilized bovine albumin standards were .01, .02, .04, .06, .08, .10 and .12 mg albumin/0.1 ml. Exactly 0.1 ml of each dilution of albumin standard was placed into a clean, dry, acid washed test tube. Similarly, 0.1 ml of bronchoalveolar lavage samples were placed in test tubes. An Oxford 0.01-0.05 ml Adjustable Sampler (Lancer, St. Louis, Missouri) was used

to transfer standard and sample volumes. Oxford Disposable Plastic Tips were employed and a new tip used after each standard or sample was added to a given test tube.

Each standard and sample tube was labeled, placed in a rack and a 2 cm by 2 cm square of Parafilm placed over the opening of the tube. An Oxford 1 to 5 ml Adjustable Sampler was used to add 5 ml of diluted dye reagent to each tube excluding saline blanks. Contents were not agitated any more than necessary because vortexing and inverting test tubes resulted in foaming. Standard and sample tubes containing reagent were allowed to set for 5 to 30 minutes.

Contents of each tube were analyzed using a Spectronic 20 Spectrophotometer (Bausch and Lomb, Rochester, New York) containing a blue bulb and without a red filter. Optical density was adjusted to 595 nm. A clean, dry, acid washed cuvette was used for standards and samples. A blue hue was imparted to the cuvette as each standard and sample was poured into the cuvette for analysis. The coloration was due to dye binding with glass and did not affect readings.

Two test tubes filled with 5.1 ml saline were designated optimum transmission blanks. Saline from each tube was poured into the cuvette, placed in the cuvette chamber and lid closed. Percentage of transmission was adjusted to 100 percent. Absorbances were calculated from mean transmission values of tube containing 0.1 ml saline plus 5 ml dye. As suggested by Mehta, (79) these absorbance values were subtracted from absorbance values calculated for standards and samples. This procedure improved accuracy by compensating for the amount of

light absorbed by dye failing to bind with soluble proteins in standards and samples.

Absorbance values for standards were used to construct a standard curve. A TI-55 calculator (Texas Instruments, Lubbock, Texas) was used to construct the curve. Standard absorbance values were entered as "x" values and standard protein concentrations (mg albumin/0.01 ml) as "y" values. The calculator provided the appropriate "y" value when given the "x" (absorbance) value of any sample.

After calculating protein concentrations for each sample, values were multiplied by 10 to convert to mg protein/ml lavage. Resulting values were multiplied by 30 ml lavage to give total protein yield in mg/gm mouse lung. Resulting values were divided by recovery factor of 0.65 to compensate for assumed recovery and expressed as mg protein/gm lung weight.

Data Processing

A Kruskal-Wallis H test for completely randomized designs was used to determine significant protein concentration elevations in protocol categories (2,80). This test is a nonparametric technique employed in comparing populations, without the need for assumptions about probability distributions of those populations. In the current experiment the null hypothesis was rejected, leading to the conclusion that a difference existed between categories. A multiple comparison procedure identified the category that was significantly different (3).

A Timex/Sinclair 1000 computer (Timex/Sinclair, Sussex, England) with 16K random access memory and a Timex/Sinclair 2040 thermal printer

calculated three flight parameters. A rocket flight program developed by Borman (76) was used to process the following:

Weight of rocket and engine	(gms)
Weight of propellant	(gms)
Drag coefficient	
Body tube external diameter	(in)
Total impulse	(N-sec)
Thrust duration	(sec)
Engine time delay	(sec)

The program generated information on altitude, velocity and acceleration for each flight from powered flight phase to the end of coast-descent phase. The program calculated updated parameter values at 0.1 second intervals totaling 89 calculations.

RESULTS

Acceleration Data

Each flight was divided into three phases. Acceleration, velocity and altitude values were calculated for beginning and end of each phase as were mean values for each phase.

Powered Flight

This phase began when the rocket lifted from the launch pad and ended at engine shutdown. Thrust times lasted approximately 1.8 seconds and total impulse was 20 Newton-seconds as seen in Table I. Drag coefficient of 0.75 was calculated by Borman (76) and assumed for each flight. Composite G_z acceleration profiles for the powered flight phase revealed that a mean of $6.22 \pm .47$ (SD) G were suddenly imposed on rocket and payload at lift-off. G decreased after the initial increase. Mean acceleration values were comparable to those sustained by humans during powered flight (8).

Differences existed in acceleration profiles of mice in the current experiment, making these profiles untraditional. Rate at which G were imposed on mice may have been greater than the rate experienced by mice aboard traditional rockets. G levels on larger rockets usually increase progressively and are sustained over periods exceeding 1.8 seconds (8). Engine thrust peaked at 0.3 second post

TABLE I
Periodic Flight Parameters for Experimental Mice

Phase	G_z (G)	Altitude (M)	Velocity (M/S)
<u>Powered Flight (0-1.8 seconds)</u>			
Lift-off	6.22±.47 (SD)	.00± .00	.00± .00
Engine Shutdown	3.09±.03 (SD)	87.46±5.18 (SD)	87.42±4.14 (SD)
<u>Coast--Ascent (1.86-6.96 seconds)</u>			
Post-Engine Shutdown	-4.05±.48 (SD)	95.98±5.57 (SD)	83.33±3.64 (SD)
Pre-Apogee	-1.00±.00 (SD)	259.73±8.23 (SD)	.50± .17 (SD)
<u>Coast--Descent (7.06-8.76 seconds)</u>			
Post-Apogee	-1.00±.00 (SD)	259.73±8.23 (SD)	-.48± .13 (SD)
Pre-Parachute	-1.12±.04 (SD)	244.52±8.09 (SD)	-17.79± .22 (SD)

launch and generated 28 Newtons. The rate at which G were imposed was critical in producing sudden transient acceleration that enabled blood column inertia to cause basilar microvascular hypervolemia (8). Mean $+G_z$ acceleration between mice were not significantly different therefore all were exposed to equivalent acceleration forces during the powered flight phase. Minor variations in $+G_z$ values at lift-off were due to variations in mouse body weights. Experimental mice had mean weights of 26.74 ± 9.06 (SD) gms, mean lengths of 160.91 ± 23.43 (SD) mm and mean widths of 35.64 ± 6.36 (SD) mm.

Mouse body weights and mean $+G_z$ accelerations were inversely related. Smaller mice were subjected to faster rates of acceleration than larger ones. Mean $+G_z$ acceleration and lung weights were also inversely related with a correlation coefficient of -0.957 and a r_{test} certainty value of 99.9 percent. All experimental lungs were subjected to the same acceleration. Mice with larger lungs may have had taller vertical hydrostatic columns that moved caudally less readily because of greater inertia. Taller columns may have exerted greater pressures on basilar juxta-alveolar vessels at rest. Animals with smaller lungs may have had shorter vertical hydrostatic columns that moved caudally more readily because of less inertia. Shorter columns may have exerted less pressure on the basilar juxta-alveolar vessels at rest. The greater pressure but greater inertia of larger animals may have been countered by lower pressures but lesser inertia of smaller animals. At the end of the powered flight phase, mean velocity was 87.42 ± 4.14 (SD) meters/second and mean altitude was 87.46 ± 5.18 (SD) meters.

Coast-Ascent

This phase began at engine shutdown and was characterized by sudden reversal of the longitudinal inertial axis as denoted by the reversal of G_z values from positive to negative as reported in Table I, p. 36. During powered flight, the inertial axis pointed caudad in response to $+G_z$ acceleration. Acceleration data generated by computer suggested that at engine shutdown the mouse may have shifted closer to the base of the nosecone. The force of the shift was ameliorated by the foam ring and disk and was assumed to be negligible. Marginal injury to the head, vertebral column or spinal cord, and pulmonary edema arising therefrom could not be ruled out.

Following engine shutdown the rocket continued gaining altitude up to 6.96 seconds post launch. At apogee, $-G_z$ levels were computed for all mice therefore normal weights were exerted cephalad. After apogee animals decelerated through some angular distance (5) prior to beginning to descend. During coast-ascent and coast-descent a tracking smoke charge allowed the flight path of the rocket to be monitored. The rocket did not undergo excessive pitching, yawing or rolling.

Coast-Descent

This phase began after the rocket had attained zero velocity at peak altitude. (See Table I, p. 36.) Following apogee, the rocket turned 180° , pointed its nosecone toward earth and began accelerating. Coast-descent lasted less than two seconds therefore acceleration did not exceed $-1.2G_z$.

An explosive in the engine jettisoned the payload compartment from the body tube thereby deploying parachute and elastic shock cord and terminating coast-descent. Payload compartment and body tube were tethered by shock cord therefore opening of the parachute reduced the descent for compartment and body tube. Pulmonary apices were dependent during descent.

Physiological Data

Animal

After being recovered, mice received Ketamine (35 mg/kg body weight). Mean volume of Ketamine administered intraperitoneally to experimental, control and sham control animals was 0.018 ± 0.006 (SD) ml. Small second doses were given to animals that emerged prematurely from anesthesia.

After excising lungs, a rating system with seven categories was used to assess lung tissue condition. Experimental lungs received a mean rating of 2.09 ± 1.38 (SD) and had petechial hemorrhages on basilar surfaces. Control lungs received a mean rating of 1.13 ± 1.13 (SD), were pink and well ventilated. Sham control lungs had petechial hemorrhages throughout and received a mean of 1.5 ± 0.55 (SD), putting them between experimentals and controls. Hyperemic regions in experimental lungs were presumed due to acceleration. Lungs with nodules, tumors or other pathologies were not lavaged. Mean weight of all lungs was 0.21 mg. No significant differences were found between lung weights of experimental, control and sham control animals. Post launch increases in experimental lung weights were not found.

Kruskal-Wallis H test revealed no significant difference in the percentage of lavage fluid recovered from all mice. The mean percentage of the total volume recovered was 81.13 ± 12.74 (SD) for controls, 82.79 ± 9.58 (SD) for experimentals and 79.00 ± 8.39 (SD) for sham controls.

Protein Assay

Significant ($p < .001$) differences in protein concentration were found between control 1.53 ± 0.8 (SD) mg/g lung and experimental 13.09 ± 8.31 (SD) mg/g lung mice as seen in Table II, p. 41. Murine protein concentrations were compared with concentrations found in other mammals. Although different species have variable protein concentrations (81) it was assumed that mammals have comparable concentrations of bronchoalveolar protein. Lavage from normal cats was analyzed. No significant differences were found between bronchoalveolar protein from murine and feline controls. A mean feline protein concentration of 2.94 mg/gm was within values found in our lab therefore murine control values were accepted as reasonable. Protein concentration of 1.53 ± 0.8 (SD) mg/gm lung for control mice was less than the concentration of 5.75 ± 4.05 (SD) mg/gm lung for sham controls.

Alternate experimental mice underwent gradual radial acceleration (5) for 15 seconds in a centrifuge and exhibited protein concentrations above control values but below experimental values. Imposing G levels gradually may have allowed blood to move into dependent lung without sudden transient increase in basilar microvascular hydrostatic pressure. Further experiments may allow alterations in the physiology of mice

TABLE II
Bronchoalveolar Protein and Fluid Content

		Protein (mg/g wet lung)	Lung (wet wt./body wt.)
Control	(n=8)	1.53±0.8 (SD)	.008±.002 (SD)
Experimental	(n=11)	13.09±8.31 (SD)*	.008±.001 (SD)
Sham	(n=6)	5.73±4.05 (SD)	.008±.001 (SD)

* $p < .001$ compared with control (Kruskal-Wallis H test followed by multiple comparisons tests).

subjected to sudden transient linear acceleration to be compared with alterations in mice subjected to gradual transient radial acceleration.

DISCUSSION

Prelaunch

Animal Stress

The role of stress in increasing bronchoalveolar protein could not be definitively ascertained. Sympathetic responses are associated with stress reactions. Sympathetic efferent nerve activity into murine pulmonary microvasculature may have resulted in release of alpha-adrenergic agonists thereby increasing endothelial junction permeability (54) before launch. Sympathetic stimulation due to handling of mice during weight and length measurements may have lead to norepinephrine mediated increases in histamine from pulmonary mast cells.

This sequence of events was avoided where possible by taking precautions to minimize animal stress. Transporting animals to launch site while confined in an open payload compartment was discontinued because it was suspected that stress was greater than if the animal was placed into the compartment immediately before launch. Protein concentration elevations in sham-control mice may have been partially attributable to the stress of restricting movement within payload compartment. Some investigators have ameliorated pulmonary damage in mammals by pretreatment with sympatholytic agents (82). Pretreatment of experimental mice with these agents may reveal crucial

information clarifying the extent to which stress may be involved in increasing protein concentrations in lavage.

Abdominal Binders. To insure that all mice were oriented to receive the same acceleration, each was placed in a plastic film canister, then placed in the payload compartment of the rocket. The canister maintained the longitudinal axis of the mouse parallel with that of the rocket. The canister also served as an abdominal binder minimizing abdominal pooling of blood thereby supporting blood pressure during acceleration. Canister dimensions were not tailored for each animal therefore binding may have been greater in larger mice.

Cephalad shift of abdominal contents, after binder application, may have been greater for larger mice. Cephalad compression of pulmonary parenchyma due to binder is well established (7). However, there were no signs of ventilatory impairment in animals with binders. Cephalad movement of the diaphragm may have increased basilar pleural pressures above basilar small airway pressures resulting in compressed small airways proximal to alveoli and trapped gas in alveoli. It has not been determined to what extent prelaunch airway collapse may have resulted in microatelectasis in dependent lung regions. It seems plausible that mice remaining in binders beyond some critical point may have experienced absorption microatelectasis with increased shunt (\dot{Q}_S/\dot{Q}_T) and deadspace ventilation (V_D/V_T) ratios resulting in hypoxemia and further stress.

It is uncertain whether binded mice experienced transpulmonary pressure increases and whether acceleration may have further increased

basilar pleural pressures resulting in widespread small airway collapse. Humans with abdominal binders experience increased basilar airway closure during increased exhaled flow rate maneuvers (7). A similar phenomenon may operate in binded mice during launch. Binders were applied for slightly more than five minutes, beginning immediately before launch and ending immediately following recovery.

Hypoxemia. Hypoxemia arising from progressive prelaunch small airway collapse may result in pulmonary arteriolar constriction, increased cardiac output, lactic acidosis and hyperventilation (59). Hypoxemia mediated constriction of arterioles may engender pulmonary arterial hypertension yielding arterial wall rupture and formation of periarterial edema cuffs (59). Periarterial acculumation of fluid and protein in presumably hypoxic lungs of experimental and sham control mice may account for some of the increases in protein found in control and sham control animals.

Hypoxic constriction of small arteries increases pulmonary vascular resistance in proportion to the hypoxemia (60). Hypoxic constriction also redistributes blood from lung bases to apices (61). Hemodynamic pressures may have been augmented by prelaunch hypoxia mediated shifts of blood into apices thereby increasing hydrostatic pressure gradients in the lung during launch. Increased pressure gradients may have resulted in greater accumulation of fluid and protein in periarterial regions of experimental mice.

Launch

Powered Flight

At lift-off, mean acceleration was $6.22 \pm .47$ (SD) $+G_z$; therefore, the average mouse was subjected to more than six times resting weight. Acceleration profiles for experimental mice were characterized by sudden rates of onset. This was different from the gradual acceleration profile for astronaut John Glenn (7). Sudden imposition of $+G_z$ acceleration and its caudally directed inertial vector upon lungs may have resulted in caudad parenchymal compression. This distortion is due to the behavior of lung tissue density within an accentuated gravitational gradient (10). At $+6.22 G_z$ there is a sixfold accentuation in murine intrapleural pressures in which apical pleural pressures become markedly negative while basilar pleural pressures become markedly positive. Sixfold changes in pulmonary vascular pressure also occur in which apical arterial and venous pressures becomes markedly negative while basilar arterial and venous pressures become markedly positive. These intrathoracic pleural and vascular pressure changes cause apical alveoli to increase in volume while basilar alveoli decrease in volume (5,8,9) during powered flight.

Increased basilar microvascular pressures during sudden $+G_z$ acceleration may have been due to hypervolemia identical to that induced by Yoneda (41) as a result of fluid overload. Evidence suggests that highly mobile blood (8) may have pooled inducing stagnant hypoxia resulting in visual, hearing and consciousness dysfunctions (11) in mice.

Although heart rates were not monitored, increased rates proportional to the level of acceleration have been reported by Burton (4). Excessive sympathetic activity may have resulted in tachycardia. In humans, accelerations greater than $+6G_z$ lasting less than 15 seconds have been known to render the myocardium ischemic as documented by S-T segment depression (4). Frequency of dysrhythmias including premature ventricular contractions (PVC) have been found to increase as acceleration levels increase from +7 to $9G_z$ (15). Dysrhythmias may have been responsible for post recovery demise of three experimental mice. In each case perinasal and perioral mucous membranes were devoid of blood. This sign suggested caudad pooling of blood with increased risk of fatal dysrhythmia.

Although sudden transient hypervolemia (28) of basilar pulmonary microvasculature may have increased intravascular hydrostatic pressure (29), stress related sympathetic responses may have led to constriction of precapillary resistance vessels (54) thereby decreasing pressure and flow in alveolar capillaries. The result may have been negligible amounts of pericapillary edema collecting within true alveolar interstitium. Mean lung wet weight/body weight ratios were 0.008 ± 0.002 (SD) for all mice as reported in Table II, p. 41.

Increased capillary pressures may have increased transvascular filtration rates leading to perimicrovascular washout of proteins. Resulting increases in osmotic pressure differences between microvascular and perimicrovascular compartments act to oppose further filtration from capillaries (46). True interstitium in mice is

proportionally smaller than in other mammals, therefore less capable of accommodating large volumes of edema (38). Fibroblasts within the interstitium are known to restrict the degree to which true alveolar interstitial spaces may widen (37). Edema in true interstitium adheres to interstitial connective tissue fibers that are part of the axial-peripheral fiber network and is quickly transported along sub-atmospheric pressure gradients to triple lines that extend to juxta-alveolar sump sites and associated lymphatic vessels (38). Evidence suggests that small increases in vascular permeability are not likely to be reflected in lung edema because lymphatic vessels quickly remove fluid and protein (62).

Leakage of fluid and protein from true interstitium of alveolar septum into alveolar air spaces via alveolar epithelium may have been minimized by structural characteristics of alveolar epithelial intercellular clefts. Tortuous zonulae occludentes comprising three to six interconnected sealing strands situated toward the adluminal side of the cleft characterize murine alveolar epithelium intercellular junctions (26). Composition of these intercellular junctions makes transport of water soluble solutes into alveolar air spaces very unlikely (25).

Microvascular hypervolemia during powered flight may have increased hydrostatic pressures (83), zone three microvascular surface area and net transvascular filtration rate (84). Unperfused lung zones regress caudally as $+G_z$ levels increase (10). Hemodynamic forces promote macromolecular transport through endothelial clefts

when endothelial junctions are subjected to pressures of 30 mm Hg (85) to 50 mm Hg (29). Schneeberger and Karnovsky (28) have reported increased mean endothelial junction widths in mice following iatrogenic hypervolemia.

Evidence suggests that edema begins around small peribronchiolar arteries (14,15,22,23,41). Endothelial cells of small arteries possess many contractile myofibrils capable of causing the cell to contract thereby increasing the radii of intercellular junctions (41). This increased permeability may have been additive considering the increased permeability that may have occurred earlier due to sympathetic stimulation (69).

Fluid and protein proceed along myoendothelial junctions found at intervals along endothelial basement membrane (43). After passing into interstitium surrounding smooth muscles, protein enters peribronchiolar space by five minutes post hypervolemia (41). Edema finds its way toward peribronchiolar connective tissue fibers, fluid sumps and lymphatic vessels (28,86). During sudden transient $+G_z$ acceleration, fluid and protein may exude from small peribronchiolar arteries, representing a regionalized increase in extravascular fluid that may evade experimental detection (69). An acceleration induced increase in net transvascular filtration rate may have resolved before laboratory assay could detect edema. Approximately 30 to 45 minutes elapsed from launch to lung lavage.

Enzymatic tracers found in intercellular clefts of murine bronchiolar epithelial cells following hypervolemia means that protein can

pass through bronchiolar clefts into lumen (41). Proteins may then have been carried distally into alveoli.

It was not ascertained whether proteins recovered were components of surfactant or of intravascular origin. Evidence so far appears to favor intravascular (74) rather than an intra-alveolar origin (71). Further studies examining the role of sudden transient $+G_z$ acceleration may have to quantitate the degree of microvascular permeability attributable to confounding factors such as interrupted blood flow and nerve supply following extraction of lungs. Excising mammalian lungs may increase microvascular permeability (64).

Coast-Ascent

Engine shutdown occurred at 1.8 seconds post launch and was characterized by a mean acceleration of $+3.09 \pm 0.03$ (SD) G_z . At 1.86 seconds the rocket began its coast-ascent and its mean acceleration changed to -4.05 ± 0.48 (SD) G_z . The start of coast-ascent reversed the acceleration vector from $+G_z$ to $-G_z$ and reversed the corresponding inertial vectors. In the interval between 1.8 and 1.86 seconds the average animal underwent a change in magnitude and direction of its weight. At 1.8 seconds the average animal weighed in excess of three times its resting weight and the weight was directed caudad. By 1.86 seconds the average animal suddenly increased to over four times its resting weight but that weight was directed cephalad.

Sudden shifts from $+G_z$ to $-G_z$ may have led to a sudden cephalad shift of blood and cerebrospinal fluid thereby initiating a transient increase in intracranial pressure (ICP). Although believed negligible,

the force with which the animal may have been sent toward the nose cone base may have increased ICP enough to engender increased vascular permeability in the lung (62). It is not known whether combined effects of neurogenically mediated increases in vascular permeability along with a shift in apical blood volume due to cephalad inertia may have played a role in furthering apical edema.

Sudden transient $-G_z$ acceleration may have induced a cephalad shift in lung parenchyma in which basilar pleural and vascular pressures became markedly negative and apical pleural and vascular pressures became markedly positive. Basilar airway and alveoli may have increased in volume while apical alveoli may have decreased, reversing conditions occurring during powered flight. At 6.96 seconds the rocket approached apogee while mean acceleration of $-1.0 G_z$ was exerted, meaning that animals were essentially standing on their heads at normal resting weight. Mean acceleration for coast-ascent was -1.68 ± 0.08 (SD) G_z and may not have been sufficient to cause physiologic alterations.

Coast-Descent

At 7.06 seconds post launch the rocket began to descend with its nose cone pointed toward earth. At 8.76 seconds the average animal underwent an acceleration of -1.12 ± 0.04 (SD) G_z , therefore the animal weighed slightly more than at rest and the weight continued to be directed cephalad. The increased weight may have been due to a tendency for the animal to accelerate slightly faster than the rocket upon which drag was acting.

Basilar pleural and vascular pressures may have remained subatmospheric further reducing airway and alveolar collapse. Apical pleural and vascular pressures may have remained positive, promoting airway and alveolar collapse. The problem of hypoxia may have continued unresolved from before launch through powered flight, coast-ascent and coast-descent. Hypoxia may have occurred due to depletion of oxygen within the payload compartment. Hypoxemia may have resulted from ventilation-perfusion (\dot{V}/\dot{Q}) mismatching during each phase of the flight.

Coast-descent ended at 8.76 seconds post launch with deployment of the parachute. Rocket aerodynamic instability after parachute deployment made analysis of the physiologic effects of recovery impossible. Padding in the payload compartment, and shock cord may have ameliorated shocks associated with deployment.

The rocket was recovered in mid-air by catching it a few feet before impact on the ground. Padding in the payload compartment prevented excessive shock.

CONCLUSION

Significantly elevated concentrations of protein were recovered from bronchoalveolar lavage of experimental mice undergoing sudden transient $+G_z$ acceleration. The acceleration may have engendered sudden transient hypervolemia in pulmonary juxta-alveolar microvessels, especially small peribronchiolar arteries.

Intravascular hydrostatic pressures may have separated maculae occludents in arterial endothelial intercellular clefts thereby encouraging exudation via myoendothelial junctions into perivascular spaces. Increased permeability may not have been sufficient to manifest as increased lung wet weight/body weight ratio or may have confounded results by resolving before its magnitude could be determined. Exudates may have passed via bronchiolar epithelial intercellular clefts into bronchiolar lumen, later descending into alveolar air spaces.

Sympathetic efferent nerve activity arising from stress before, during and after launch may have decreased the threshold of arterial endothelial permeability prior to the hypervolemia of acceleration.

Hypoxia associated with abdominal constriction and with payload compartment oxygen depletion may have increased vasoconstriction of small arteries rendering alveolar capillaries of negligible importance in contributing to acceleration mediated hemodynamic pulmonary edema.

The triad of hyperpermeability, hypoxia and hypervolemia may account for migration of protein into airways and alveoli. Definitive answers regarding route followed by proteins presumed to be of intravascular origin may have to await electron micrographic study of mouse lungs into whose intravascular compartment enzymatic tracers have been injected prior to sudden transient $+G_z$ acceleration.

Sudden transient $+G_z$ acceleration may be fundamentally different from traditional gradual acceleration profiles for rockets. Sudden transient $+G_z$ acceleration may represent a mechanism by which hemodynamic pulmonary edema may be reliably induced in murine pulmonary microvasculature allowing acceleration mediated perivascular edemagenesis to be studied in detail.

APPENDICES

APPENDIX A
TYPED ROCKET FLIGHT PROGRAM

TYPED ROCKET FLIGHT PROGRAM

```
10 SLOW
20 PRINT TAB 2; "*****"
30 PRINT TAB 2; "  ROCKET FLIGHT PROGRAM  "
40 PRINT TAB 2; "*****"
50 REM  M. BORMAN
60 PRINT
70 PRINT "ENTER ROCKET NAME:  ";
80 INPUT N$
90 PRINT N$
100 PAUSE 60
110 LPRINT
120 LPRINT
130 PRINT "ENTER ENGINE TYPE:  ";
140 INPUT E$
150 PRINT E$
160 PAUSE 60
170 LPRINT
180 LPRINT
190 PRINT "ENTER ENGINE WT. OF ROCKET AND ENGINE"
200 PRINT "(IN GRAMS):  ";
```

```
210 INPUT W
220 PRINT W
230 PAUSE 60
240 LET W=W*.035
250 LPRINT
260 LPRINT
270 PRINT "ENTER PROPELLANT WT. (GR.): ";
280 INPUT WP
290 PRINT WP
300 PAUSE 60
310 LET WP=WP*.035
320 LPRINT
330 LPRINT
340 PRINT "ENTER DRAG COEFFICIENT: ";
350 INPUT CD
360 PRINT CD
379 PAUSE 60
380 LPRINT
390 LPRINT
400 PRINT "ENTER ROCKET DIAM. (IN): ";
410 INPUT RD
420 PRINT RD
430 PAUSE 60
440 LPRINT
450 LPRINT
```

```
460 PRINT "ENTER TOTAL IMPULSE (N-SEC): ";
470 INPUT TI
480 PRINT TI
490 PAUSE 60
500 LET TI=TI*.225
510 LPRINT
520 LPRINT
530 PRINT "ENTER THRUST DURATION (SEC): ";
540 INPUT TL
550 PRINT TL
560 PAUSE 60
570 LPRINT
580 LPRINT
590 PRINT "ENTER ENGINE TIME DELAY (SEC): ";
600 INPUT TD
610 PRINT TD
620 PAUSE 60
630 LPRINT
631 COPY
641 LPRINT AT 21,0; "ROCKET NAME:";N$
650 SCROLL
660 LPRINT AT 21,0; "ENGINE TYPE:";E$
670 SCROLL
681 LPRINT AT 21,0
690 SCROLL
```

```
700 LPRINT AT 21,0; TAB 1;"TIME";TAB 7;"ALT";TAB 14;"VEL";TAB 25;"ACC"
710 SCROLL
720 LPRINT AT 21,0;TAB 1;"(SEC)";TAB 7;"(M)";TAB 12;"(M/SEC)";TAB 23;
    "(GEES)"
730 SCROLL
740 LPRINT AT 21,0;"-----"
750 SCROLL
769 LPRINT AT 21,0
770 SCROLL
780 LET WA=W-(.5*WP)
790 LET A=PI*(RD/2)**2
800 LET B=(W-(.5*WP))/(CD*A)
810 LET T=(TI/TL)*16
820 LET ADF=(T/WA)-1
830 FOR F=0 TO (TL+.1) STEP .1
840 FAST
850 LET TS=F
860 LET Y1=.36981*SQR (ADF/B)*TS
870 LET X=(EXP Y1+EXP (-Y1))/2
880 LET ST=235.26*B*LN X
890 LET Y=(EXP Y1-EXP (-Y1))/(2*X)
900 LET VT=87*SQR (B*ADF)*Y
910 LET D=.0001321*CD*A*(VT**2)
920 LET ACC=((T-D)/WA)-1
930 LET STP=(INT (ST*3.03+.5))/10
```

```
940 LET VTP=(INT (VT*3.03+.5))/10
950 LET ACC=(INT (ACC*10+.5))/10
960 SLOW
970 LPRINT AT 21,0;TAB 2;TS;TAB 7;STP;TAB 14;VTP;TAB 24;ACC
980 SCROLL
990 NEXT F
1000 LET T=0
1010 LET TS=0
1020 LET B=(W-WP)/(CD*A)
1030 LET VB=VT
1040 LET SC=117.63*B*LN (1+VB**2/(7569.386*B))
1050 LET TC=2.7041*SQR B*ATN (VB/(87.0*SQR B))
1060 FOR F=0.1 TO TD STEP .1
1070 FAST
1080 LET TS=F
1090 LET N=.36981*((TC-F)/SQR B)
1100 LET SCT=SC+235.26*B*LN (COSN)
1110 LET TA=SCT+ST
1120 LET VC=87.0*SQR B*TAN N
1130 LET D=.0001321*CD*A*(VC*VC)
1140 LET ACC=((T-D)/(W-WP))-1
1150 LET TA=(INT (TA*3.03+.5))/10
1160 LET VC=(INT (VC*3.03+.5))/10
1170 LET ACC=(INT (ACC*10+.5))/10
1180 SLOW
```

1190 LPRINT AT 21,0;TAB 2;TS+TL;TAB 7;TA;TAB 14;VC;TAB 24;ACC
1200 SCROLL
1210 NEXT F
1211 LPRINT
1212 LPRINT
1213 LPRINT "=====
1214 LPRINT "PARACHUTE DEPLOYMENT"
1215 LPRINT "=====
1216 LPRINT
1220 LPRINT "THIS REPORT HAS BEEN PRODUCED"
1230 LPRINT "BY TIMEX/SINCLAIR 1000/2040"
1240 LPRINT "COMPUTER SYSTEM."
1250 LPRINT
1260 LPRINT
1270 LPRINT "CARDIOPULMONARY AERONAUTICS"
1280 LPRINT "RESEARCH PROJECT."
1290 LPRINT
1300 LPRINT
1310 LPRINT "CRITTENDEN"
1320 LPRINT "GUTIERREZ"
1330 LPRINT "DUKESHERER"
1340 LPRINT
1350 LPRINT
1360 LPRINT "UNIV. OF CENTRAL FLORIDA"
1370 LPRINT "RESPIRATORY THERAPY PROGRAM"

1380 LPRINT "CARDIOPULMONARY RESEARCH LAB"

1390 LPRINT

1400 LPRINT

1410 LPRINT

1420 LPRINT "END"

1430 LPRINT

1440 LPRINT

1450 LPRINT

APPENDIX B
DATA SHEET

CARDIOPULMONARY AERONAUTICS RESEARCH PROJECT--DATA SHEET

University of Central Florida
College of Health
Respiratory Therapy Program
Cardiopulmonary Research Lab

Investigator(s) _____ Date _____

°PREFLIGHT ANIMAL DATA

Mouse Number _____ Mouse Sex _____

Mouse Length _____ Mouse Width _____

Mouse Color _____ Other Characteristics _____

Research Protocol Category [Circle One] C (Control), SC (Sham
Control), E (Experimental), AE (Alternate Experimental)

Physical Examination Findings: _____

°PREFLIGHT ATMOSPHERIC DATA

Current Wind Speed (MPH) _____ Current Wind Direction _____

Humidity (in Hg) _____ Forecast _____

°PREFLIGHT LAUNCH VEHICLE AND ENGINE DATA

Launch Date _____ Launch Time _____

Launch Vehicle Name _____ Flight Number _____

Hardware Inspection Findings _____

Engine Type _____ Engine Weight (gm) _____
 Propellant Weight (gm) _____ Total Impulse (N-sec) _____
 Thrust Duration (sec) _____ Engine Time Delay (sec) _____

Weight of Launch Vehicle (including):

1. Engine (gm) _____
2. Mouse (gm) _____
3. Body Tube, Payload Compartment and Nose Cone (gm) _____
4. Parachute, Brass Swivel and Recovery Wadding (gm) _____
5. Plastic Animal Restraining Cannister (PARC) (gm) _____
6. Miscellaneous: Shock Cord, Foam Disc, etc. (gm) _____

Total (gm) _____

Drag Coefficient _____

Launch Vehicle Outer Diameter (in) _____

°FLIGHT OBSERVATIONS

°POST FLIGHT ANIMAL DATA

Physical Examination Findings _____

Anesthetic Name _____ Dose (mg/kg) _____

Injection Volume (ml) _____ Injection Site _____

Time of Injection _____

°LABORATORY DATA (SURGERY)

Time Elapsed from Recovery of Launch Vehicle
to Surgery _____ Hr. _____ Min.

Surgical Notes _____

In Situ Gross Pulmonary Rating [Circle One]

- (0) Pink, Well Ventilated Lungs Without Evidence of Pathologic Alterations
- (1) Petechial Hemorrhages Cover 10-33% of Pulmonary Parenchymal Surface
- (2) Petechial Hemorrhages cover 33-66% of Pulmonary Parenchymal Surface
- (3) Petechial Hemorrhages cover 66-99% of Pulmonary Parenchymal Surface
- (4) Evidence of Tumors, Muroid Nodules, Pneumonic Processes, etc.
- (5) Evidence of Hematomas, Atelectasis, Closed Pneumothorax, etc.
- (6) Bilateral Hyperemic Hepatization with Pulmonary Edema at Trachea

Wet Lung Weight (gm) _____

Negative Evacuation Pressure Applied to Lungs (in Hg) _____

	In	Out	Qtts
1st Alveolar-Endobronchial Lavage (ml)	_____	_____	_____
2nd Alveolar-Endobronchial Lavage (ml)	_____	_____	_____
3rd Alveolar-Endobronchial Lavage (ml)	_____	_____	_____

Total Volume Recovered (ml) _____

Lavage Storage Bottle Number _____

Time Elapsed from Vehicle Recovery to Icing of Bottled
Lavage _____ Hr. _____ Min.

°LABORATORY DATA (SPECTROPHOTOMETRIC ANALYSIS)

Protein Concentration (mg/gm lung) _____

°LABORATORY DATA (COMPUTER CALCULATIONS)

Mean $+G_z$ (Powered Flight Phase) (g) _____Mean $+G_z$ (Coast-Ascent Phase) (g) _____Mean $+G_z$ (Coast-Descent Phase) (g) _____

Maximum Velocity (Powered Flight Phase) (m/sec) _____

Maximum Altitude (Powered Flight Phase) (m) _____

LITERATURE CITED

1. Flanagan, D. Space flight. Sci. Am. 186:38; 1952.
2. McClave, J.T.; Dietrich, F.H., editors. Kruskal-Wallis H test for a completely randomized design. Statistics. 2d ed. San Francisco: Dellen Publishing Co.; 1982: 452-457.
3. Daniel, W.W., editor. Multiple comparisons. Applied nonparametric statistics. Boston: Houghton Mifflin Co.; 1978: 211-214.
4. Burton, R.R.; Leverett, S.D.; Michaelson, E.D. Man at high sustained +G_z acceleration: a review. Aerosp. Med. 45:1115-1136; 1974.
5. Lindberg, E.F.; Wood, E.H. Acceleration. Brown, J.H.U. ed. Physiology of man in space. New York: Academic Press; 1963: 61-111.
6. Rogers, T.A. The physiological effects of acceleration. Sci. Am. 206:61-70; 1962.
7. Glazier, J.D.; Hughes, J.M.B. Effect of acceleration on alveolar size in the lungs of dogs. Aerosp. Med. 39:282-288; 1968.
8. Wood, E.H.; Nolan, A.C.; Donald, D.E.; Cronin, L. Influence of acceleration on pulmonary physiology. Fed. Pro. 22:1024-1034; 1963.
9. Vandenberg, R.A.; Nolan, A.C.; Reed, J.H.; Wood, E.H. Regional pulmonary arterial-venous shunting caused by gravitational and inertial forces. J. Appl. Physiol. 25:516-527; 1968.
10. Glaister, D.H. Effects of acceleration on pulmonary blood flow. Fishman, A.P.; Hecht, H.H. eds. Pulmonary circulation and interstitial space. Chicago: Univ. of Chicago Press; 1968: 391-408.
11. Wood, E.H.; Lambert, E.H.; Baldes, E.J.; Code, C.F. Effects of acceleration in relation to aviation. Fed. Pro. 5:327; 1946.
12. Laughlin, M.H.; Witt, W.M.; Whittaker, R.N. Regional cerebral blood flow in conscious miniature swine during high sustained +G_z acceleration stress. Aviat. Space Environ. Med. 50: 1129-1133; 1979.

13. Bjurstedt, H.G.; Rosenhamer, G.; Tyden, G. Gravitational stress and autonomic cardiac blockage. Acta Physiol. Scand. 96: 521-531; 1976.
14. Matalon, S.U.; Farhi, L.E. Cardiopulmonary readjustment in passive tilt. J. Appl. Physiol. 47:503-507; 1979.
15. Shubrooks, S.J. Changes in cardiac rhythm during sustained high levels of positive (+G_Z) acceleration. Aerosp. Med. 43:1200-1206; 1972.
16. West, J.B.; Dollery, C.T.; Naimark, A. Distribution of blood flow in isolated lung: relation to vascular and alveolar pressures. J. Appl. Physiol. 19:713-724; 1964.
17. Banister, J.; Torrance, R.W. The effects of the tracheal pressure upon flow: pressure relations in the vascular bed of isolated lungs. Quart. J. Exptl. Physiol. 45:352-367; 1960.
18. Comroe, J.H., editor. Respiratory adjustments in health. Physiology of respiration. 2d ed. Chicago: Year Book Medical Publ.; 1974: 253-254.
19. Jones, J.G.; Clarke, S.W.; Glaister, D.H. Effect of acceleration on regional lung emptying. J. Appl. Physiol. 26:827-832; 1969.
20. Hughes, J.M.B.; Glazier, J.B.; Maloney, J.E.; West, J.B. Effect of lung volume on the distribution of pulmonary blood flow in man. Respir. Physiol. 4:58-72; 1968.
21. Glaister, D.H., editor. The effects of gravity and acceleration on the lung. Slough, England: Technivision Services; AGARDograph Number 133: 121-149; 1970.
22. Cottrell, T.S.; Levine, O.R.; Senior, R.M.; Wiener, J.; Spiro, D.; Fishman, A.P. Electron microscope alterations at the alveolar level in pulmonary edema. Circ. Res. 6:783-797; 1967.
23. Staub, N.C.; Nagano, H.; Pearce, M.L. Pulmonary edema in dogs, especially the sequence of fluid accumulation in lungs. J. Appl. Physiol. 22:227; 1967.
24. Claude, P.; Goodenough, D.A. Fracture faces of zonulae occludentes from "tight" and "leaky" epithelia. J. Cell Biol. 58:390-400; 1973.
25. Schneeberger, E.E.; Karnovsky, M.J. Substructure of intercellular junctions in freeze-fractured alveolar-capillary membranes of mouse lung. Circ. Res. 38:404-411; 1976.

26. Schneeberger-Keeley, E.E.; Karnovsky, M.J. The ultrastructural basis of alveolar-capillary membrane permeability to peroxidase used as a tracer. J. Cell Biol. 37:781-793; 1968.
27. Staehelin, L.A.; Hull, B.E. Junctions between living cells. Sci. Am. 238:140-152; 1978.
28. Schneeberger, E.E.; Karnovsky, M.J. The influence of intravascular fluid volume on the permeability of newborn and adult mouse lungs to ultrastructural protein tracers. J. Cell Biol. 49:319-334; 1971.
29. Pietra, G.G.; Szidon, J.P.; Leventhal, M.M.; Fishman, A.P. Hemoglobin as a tracer in hemodynamic pulmonary edema. Science 166:1643-1646; 1969.
30. Glazier, J.B.; Hughes, J.M.B.; Maloney, J.E.; West, J.B. Measurements in capillary dimensions and blood volume in rapidly frozen lungs. J. Appl. Physiol. 26:65; 1969.
31. Visscher, M.B.; Haddy, F.J.; Stephens, G. The physiology and pharmacology of lung edema. Pharm. Rev. 8:389-434; 1956.
32. Simonescu, N.; Simonescu, M.; Palade, G.E. Open junctions in the endothelium of the post capillary venules of the diaphragm. J. Cell Biol. 79:27-44; 1978.
33. White, A.; Handler, P.; Smith, E.L., editors. Blood. Principles of biochemistry. 4th ed. New York: McGraw-Hill Book Co.; 1968: 709-710.
34. Karnovsky, M.J. Ultrastructural basis of capillary permeability studies with peroxidase as a tracer. J. Cell Biol. 35:213; 1967.
35. Gruneberg, H. The growth of the blood of the suckling mouse. J. Pathol. Bacteriol. 22:323-329; 1941.
36. Karrer, H.E. The ultrastructure of mouse lung. J. Biophys. Biochem. Cytol. 2:241-252; 1956.
37. Weibel, E.R.; Bachofen, H. Structural design of the alveolar septum and fluid exchange. Fishman, A.P.; Renkin, E. eds. Pulmonary edema. Baltimore: Am. Physiol. Soc.; 1979: 1020.
38. Weibel, E.R. The ultrastructure of the alveolar-capillary membrane or barrier. Fishman, A.P.; Hecht, H.H. eds. The pulmonary circulation and interstitial space. Chicago: Univ. of Chicago Press; 1968: 9-27.

39. Weibel, E.R. Design and structure of the human lung. Fishman, A.P. ed. Assessment of pulmonary function. New York: McGraw-Hill; 1980: 18-65.
40. Kapanci, Y.; Assimacopoulos, A.; Zwahlen, A.; Irle, C.; Gabbiani, G. "Contractile interstitial cells" in pulmonary alveolar septa. J. Cell Biol. 60:375-392; 1974.
41. Yoneda, K. Anatomic pathway of fluid leakage in fluid overload pulmonary edema in mice. Am. J. Pathol. 101:7-16; 1980.
42. Kuhn, C. Cells of the lung and their organelles. Crystal, R.G. ed. The biochemical basis of pulmonary function. New York: Marcel Dekker, Inc.; 1976: 3-48.
43. Rhodin, J.A.G., editor. Cardiovascular system. An atlas of histology. New York: Oxford Univ. Press; 1975: 190-208.
44. Vreim, C.E.; Snashall, P.D.; Demling, R.H.; Staub, N.C. Lung lymph and free interstitial fluid protein composition in sheep with edema. Am. J. Physiol. 230:1650-1653; 1976.
45. Erdmann, A.J.; Vaughan, T.R.; Brigham, K.L.; Woolverton, W.C.; Staub, N.C. Effect of increased vascular pressure on lung fluid balance in unanesthetized sheep. Circ. Res. 37:271-284; 1975.
46. Crandall, E.D.; Staub, N.C.; Goldberg, H.S.; Effros, R.M. Recent developments in pulmonary edema. Ann. Int. Med. 99:808-822; 1983.
47. Sprung, C.L.; Rackow, E.C.; Fein, I.A.; Jacob, A.I.; Isikoff, S.K. The spectrum of pulmonary edema: differentiation of cardiogenic, intermediate, and non-cardiogenic forms of pulmonary edema. Amer. Rev. Respir. Dis. 124:18-22; 1981.
48. Staub, N.C. Pulmonary edema due to increased microvascular permeability to fluid and protein. Circ. Res. 43:143-151; 1978.
49. Taylor, A.E., Parker, J.C., Kviety, P.R.; Perry, M.A. The pulmonary interstitium in capillary exchange. Ann. NY Acad. Sci. 384:146-165; 1982.
50. Pietra, G.G.; Szidon, J.P.; Callahan, E.J.; Fishman, A.P. Permeability of the alveolo-capillary membrane to proteins. J. Clin. Invest. 50:73a; 1971.
51. Gee, M.H.; Staub, N.C. Role of bulk fluid flow in protein permeability of the dog lung alveolar membrane. J. Appl. Physiol. 42:144-149; 1977.

52. Weisman, S.J. Edema and congestion of the lungs resulting from intracranial hemorrhage. Surgery 6:722-729; 1939.
53. Beckman, D.L. Rat lung hyper-reactivity to stress. Aviat. Space Environ. Med. 49:70-72; 1978.
54. Fillenz, M. Innervation of pulmonary and bronchial blood vessels of the dog. J. Anat. 106:449-461; 1970.
55. Grimm, D.J.; Dawson, C.A.; Hakim, T.S.; Linehan, J.H. Pulmonary vasomotion and the distribution of vascular resistance in a dog lung lobe. J. Appl. Physiol. 45:545-550; 1978.
56. Theodore, J.; Robin, E.D. Speculation on neurogenic pulmonary edema. Amer. Rev. Respir. Dis. 133:405-411; 1976.
57. Tong, E.Y.; Mathe', A.A.; Fisher, P.W. Release of norepinephrine by sympathetic nerve stimulation from rabbit lungs. Am. J. Physiol. 235:803-808; 1978.
58. Beckman, D.L.; Mason, K.F.; Bean, J.W. Sympathetic factors in acute pulmonary injury. Chest 65:385-405; 1974.
59. Whayne, T.F.; Severinghaus, J.W. Experimental hypoxic pulmonary edema in the rat. J. Appl. Physiol. 25:729-732; 1968.
60. Von Euler, U.S.; Liljestrand, G. Observations on the pulmonary arterial pressure in the cat. Acta Physiol. Scand. 12:301-306; 1946.
61. Neumann, P.H.; Kivlen, C.M.; Johnson, A.; Minnear, F.L.; Malik, A.B. Effect of alveolar hypoxia on regional pulmonary perfusion. J. Appl. Physiol. 56:338-342; 1984.
62. Staub, N.C. Pulmonary edema. Physiol. Rev. 54:678-811; 1974.
63. Fry, D.L. Acute vascular endothelial changes associated with increased blood velocity gradients. Circ. Res. 22:165-197; 1968.
64. Morriss, A.W.; Drake, R.E.; Gabel, J.C. Comparison of microvascular filtration characteristics in isolated and intact lungs. J. Appl. Physiol. 48:438-443; 1980.
65. Fisher, A.B.; Dodia, C.; Linask, J. Perfusate composition and edema formation in isolated rat lungs. Exper. Lung Res. 1:13-21; 1980.
66. Reynolds, R.W. Pulmonary edema as a consequence of hypothalamic lesions in rats. Science 141:930-932; 1963.

67. Luisada, A.A. Mechanisms of neurogenic pulmonary edema. Am. J. Cardiol. 20:66-72; 1967.
68. Cameron, G.R.; De, S.H. Experimental pulmonary edema of nervous origin. J. Pathol. Bacteriol. 61:375-387; 1949.
69. Van Der Zee, H.; Malik, A.B.; Lee, B.C.; Hakim, S. Lung fluid and protein exchange during intracranial hypertension and the role of sympathetic mechanisms. J. Appl. Physiol. 48:273-280; 1980.
70. Aston, R.; Roberts, V.L. The effects of drugs on vibration tolerance. Arch. Int. Pharmacodyn. 55:289-299; 1965.
71. Sueishi, K.; Tanaka, K.; Oda, T. Immunoultrastructural study of surfactant system. Lab. Invest. 37:136-142; 1977.
72. Hurst, D.J.; Kilburn, K.H.; Lynn, W.S. Isolation and surface activity of soluble alveolar components. Respir. Physiol. 17: 72-80; 1973.
73. Scarpelli, E.M.; Chang, S.J.; Colacicco, G. A search for the surface active pulmonary lipoprotein. Amer. Rev. Respir. Dis. 102:285-289; 1970.
74. Reifenrath, R.; Zimmerman, I. Blood plasma contamination of the lung alveolar surfactant obtained by various sampling techniques. Respir. Physiol. 18:238-248; 1973.
75. Fertig, D.S.; Edwards, V.W. The physiology of the house mouse. Sci. Am. 221:103-110; 1969.
76. Borman, M. Model rocket flight: a program for the Timex/Sinclair 1000. Model Rocketeer. J. Natl. Assn. Rocketry 25:14; 1983.
77. Oyarzun, M.; Clements, J.A. Ventilatory and cholinergic control of pulmonary surfactant in the rabbit. J. Appl. Physiol. 43: 39-45; 1977.
78. Fazekas De St. Groth, S.; Webster, R.G.; Datyner, A. Two new staining procedures for quantitative estimation of proteins on electrophoretic strips. Biochim. Biophys. Acta 71:377-391; 1963.
79. Mehta, P. Personal communication.
80. Malone, L. Personal communication.

81. Shelley, S.H.; Paciga, J.E.; Balis, J.U. Species differences in the composition of lung surfactant. Fed. Proc. 40:796; 1976.
82. Beckman, D.L.; Bean, J.W.; Baslock, D.R. Sympathetic influence on lung compliance and surface forces in head injury. J. Appl. Physiol. 30:394-399; 1971.
83. Maloney, J.E.; Bergel, D.H.; Glazier, J.B.; Hughes, J.M.B.; West, J.B. Effect of pulsatile pulmonary artery pressure on distribution of blood flow in isolated lung. Respir. Physiol. 4:154-167; 1968.
84. Pappenheimer, J.R.; Soto-Rivera, A. Effective osmotic pressure of the plasma proteins and other quantities within the capillary circulation in the hindlimbs of cats and dogs. Am. J. Physiol. 152:471-491; 1948.
85. Nicolaysen, G.; Waaler, B.H.; Aarseth, P. On the existence of stretchable pores in the exchange vessels of the isolated rabbit lung preparation. Lymphology 12:201-207; 1979.
86. Lauweryns, J.N. The juxta-alveolar lymphatics in human adult lung. Amer. Rev. Respir. Dis. 102:877-885; 1970.